Next Nanotechnology 7 (2025) 100125

Contents lists available at ScienceDirect

Next Nanotechnology

journal homepage: www.sciencedirect.com/journal/next-nanotechnology

Research article

Photoelectrochemical CO_2 reduction on CuO-Cu_2O nanocomposites with noble metal co-catalysts enhances the production of C_1 oxygenates and acetate

Tahereh Mokary Yazdely, Ricard Garcia-Valls, Alberto Puga *

Department of Chemical Engineering, Universitat Rovira i Virgili, Av. Països Catalans 26, Tarragona 43007, Spain

ARTICLE INFO

Keywords:
Carbon dioxide
Methanol
Acetate
Heterojunction
Copper oxides
Solar fuels
Electrocatalysis

ABSTRACT

Multi-junction copper oxide nanocomposite photocathodes formed by CuO nanowire arrays coated with Cu_2O nanopyramids or stacked nanoprisms, *i.e.* CuO(NWA)|Cu_2O(NPy), exhibit remarkable electrochemical stability toward reductive corrosion. Whilst bare CuO nanowires are extremely prone to decomposition even at the mildest potentials applied, the core@shell morphology of CuO(NWA)|Cu_2O(NPy) resists cathodic potentials up to −0.7 V (*vs.* AgCl/Ag). Precisely controlled electrodeposition of silver or gold nanoparticles resulted in Ag nanotrails arranged on flatter surface regions in CuO(NWA)|Cu_2O(NPy)|Ag, whereas Au nanoaggregates were deposited on both flat areas and prominent apexes in CuO(NWA)|Cu_2O(NPy)|Au. Photocurrent measurements demonstrated redox process activation, namely above three-fold current density increases, by light for CuO(NWA)|Cu_2O(NPy). The participation of CO_2 in them was also confirmed by around 70 % photocurrent increases (higher than 0.2 mA cm^{-2}) and by sensibly milder cathodic potential onsets ($\leq$ −0.4 V), as recorded by linear sweep voltammetry. Photoelectrochemical CO_2 reduction experiments under simulated sunlight yielded oxygenated products in the liquid phase, chiefly formate, although acetate was also consistently produced, especially in the presence of noble metal co-catalysts. Specifically, acetate yields increased by 30–40 % for CuO(NWA)|Cu_2O(NPy)|Ag and CuO(NWA)|Cu_2O(NPy)|Au up to 56 and 54 μM, respectively. Methanol could be also formed under specific conditions. A mechanistic proposal is postulated to account for all stability and selectivity phenomena observed.

1. Introduction

The transformation of carbon dioxide into fuels, chemicals and materials is becoming a key avenue in the context of decarbonisation strategies and circular economy schemes [1]. Prospects of upcycling CO_2 are particularly relevant in the context of offsetting emissions, and hence, contributing to the mitigation of its daunting climate change effects [2]. Truly sustainable and renewable pathways in this regard entail capturing CO_2, either airborne or from point emission sources, and converting it using green hydrogen as the reducing agent. The economic balance of such hydrogenation processes is severely affected by the costs of both CO_2 capture and green H_2 production. The latter process generally requires renewable electricity generation and subsequent water electrolysis [3]. Moreover, most CO_2 hydrogenation processes currently considered on an industrial scale are performed via catalytic reactions at relatively high temperatures [4].

In contrast to thermochemical processes, electrochemical alternatives are technologically less developed, despite their main advantages of bypassing hydrogen production and enabling the one-step conversion of CO_2 by direct use of renewable electricity [5]. A wide range of products, spanning from C_1 to multi-carbon substances, and from alkanes to complex oxygenates, can be obtained by electrochemical CO_2 reduction [6]. However, activation of carbon dioxide may require high overpotentials, owing to its chemical stability and to the complex mechanisms entailing multiple e^-/H^+ transfer steps. One approach to further promote conversion, inspired by natural photosynthesis, involves the use appropriate light-responsive materials under irradiation [7,8]. Beyond purely photocatalytic processes, which tend to result in low productivities [9], the integration of a photocatalyst into electrochemical devices provides a hybrid technology combining light activation and enhanced electron migration, with the possibility of applying an electrical bias [10].

* Corresponding author.
E-mail addresses: tahereh.mokary@urv.cat (T. Mokary Yazdely), ricard.garcia@urv.cat (R. Garcia-Valls), alberto.puga@urv.cat (A. Puga).

https://doi.org/10.1016/j.nxnano.2024.100125
Received 9 August 2024; Received in revised form 25 November 2024; Accepted 10 December 2024
Available online 18 December 2024

Among a range of catalysts, the family of copper-based materials has a proven success record in both electrochemical [11,12] and photoelectrochemical (PEC) CO_2 reduction [13–15]. Regarding photoactivity, copper oxides, namely CuO and Cu_2O, are p-type semiconductors that can be activated under visible light owing to their narrow bandgaps (1.9–2.2 and 1.3–1.6 eV, respectively) [14]. An additional benefit of cuprous oxide lies in its relatively high conduction band, suitably positioned for challenging reduction reactions such as those required for CO_2 conversion [16]. Combinations of these favourable properties has made Cu_2O a robust and reliable component of photocathodes for CO_2 reduction into useful products [17]. The most common of such products is formic acid (or formate), which can be obtained effectively on Cu_2O photocathodes in aqueous electrolytes [18–21]. The possibility of producing CO or syngas from similar systems has also attracted attention [18,22,23]. More extensive reduction by multiple electron/proton transfer steps is also sought in research given the possibility to obtain valuable oxygenates, among which, alcohols such as methanol hold a prevalent position [24–27]. A further and ultimate intensely pursued endeavour entails the generation of multi-carbon products, chiefly ethanol and higher alcohols [28,29], or carboxylic species such as acetic acid [30–34].

Despite these enticing attributes, the use of copper oxide materials is often hampered by (photo)corrosion events during (photo)electrochemical operation, most often by over-reduction, leading to poor stability and decreased catalytic activity [35,36]. To solve these drawbacks, the design and preparation of nanostructures with well-defined morphologies and facet exposure have been adopted, given the possibility to channel electrons away from sensitive copper species [36]. Another common strategy involves the formation of heterojunction nanocomposites with other semiconductors [37–39], or Cu_2O|CuO phase-junctions [40–42]. Charge carrier transfer across heterojunction interfaces can be a successful strategy to enhance stability of copper phases by favourable redistribution of electrons and holes. Establishing semiconductor junctions with a high-aspect ratio, that is, 1D nanostructures such as nanowires or nanorods, facilitates charge diffusion along their longer direction while minimizing diffusion layer thickness across the interfaces [43,44]. Heterojunction materials including copper oxides have been the focus of photocathode design for CO_2 reduction into C_1 and C_2 oxygenated substances, owing to the suitability of copper active sites to promote partial deoxygenation and coupling reactions [14,30,33,45].

Thermally grown Cu_2O|CuO phase-junctions consistent of an outer CuO nanowire array (NWA) on the surfaces of Cu_2O interlayers can be readily produced by aerobic oxidation of metallic copper surfaces [46,47]. These nanocomposites exhibit remarkable electrochemical stability and promising photoelectrocatalytic CO_2 reduction activity [47]. Further improvements can be achieved by incorporating metallic species on the outer surface owing to a combination of electron sink properties, co-catalytic activity and selectivity, or plasmonic promotion of electron transfer [31,40,48,49]. Noble metal nanoparticles are especially interesting in this regard given their robustness and stability, and their incorporation as co-catalysts onto heterojunction nanocomposite materials based on copper oxides has led to successful photoelectrochemical CO_2 reduction into acetate, methanol and other oxygenates [26,28,30–33]. Nevertheless, Cu_2O|CuO|*M* (*M*: noble metal) photocathodes remain scarcely investigated. In this context, a dedicated endeavour on material design has been undertaken aiming at controlling noble metal loading extent and pattern, by precisely adjusting electrodeposition conditions, and in turn, minimising production costs, and preserving light exposure onto copper oxides and productivity of valuable oxygenated products. In short, this work explores the design and testing of CuO|Cu_2O multi-junction nanocomposite photocathodes for CO_2 reduction under simulated sunlight, and the promotion effects of noble metal (*i.e.* Ag, Au) on yields and selectivity. Enhancement in acetate or methanol production over the major formate product is evaluated and rationalised with respect to irradiation or to the presence of co-catalysts.

2. Experimental section

2.1. Materials

Cu sheets (thickness ≈ 0.35 mm, were supplied by RS PRO. Sodium hydroxide (≥98 %) was supplied by Fisher Scientific. Copper(II) sulfate pentahydrate silver nitrate (≥99 %, ACS reagent), hydrogen tetrachloroaurate(III) trihydrate (≥99.9 % trace metal basis), potassium bicarbonate (≥99.50 %), potassium hydrogenphthalate (BioXtra, ≥99.95 %) and deuterium oxide (99.9 atom% D) were supplied by Sigma-Aldrich. L-(+)-Lactic acid (88–92 %, Pharmpur®) was supplied by Scharlab. Carbon dioxide (99.995 %) was supplied by Carburos Metálicos. All chemicals were used as received. Milli-Q® water (18.25 MΩ cm) was used for all electrochemical procedures.

2.2. Preparation of Cu-based photoelectrodes

Hybrid CuO-Cu_2O nanocomposite photocathode materials were prepared by adapting previously reported synthetic routes. The procedure consists of two steps, that is, a simple thermal oxidation of copper sheets under static air atmosphere to generate CuO nanowire arrays (NWA) [46,47,50,51], followed by cathodic electrodeposition of Cu_2O nanopyramids (NPy) [52,53]. Further loading with noble metal co-catalysts was also performed by electrodeposition.

2.2.1. Preparation of cupric oxide nanowire arrays, CuO(NWA)

Copper sheets (1 × 2 cm) were polished, and subsequently washed by ultrasonication in acetone, isopropyl alcohol, deionized water, aqueous hydrochloric acid (1 M), again with deionized water, and finally dried under flowing nitrogen gas. The sheets were oxidized in alumina crucibles in a muffle furnace by thermal treatment under static air (heating rates *ca.* 6, 12, or 25 °C/min; then isothermally at 400 or 500 °C for 3 h), and finally allowed to cool down to room temperature. The obtained CuO(NWA) plates exhibited dark grey colour.

2.2.2. Electrodeposition of cuprous oxide nanopyramids, Cu_2O(NPy)

In a typical procedure, CuO(NWA) (or Cu sheets pre-treated as described above) were used as cathodes for Cu_2O electrodeposition, whereas platinum plate (1 cm^2) and Ag/AgCl (Metrohm) were used as counter and reference electrodes, respectively, in a one-compartment three-electrode cell. The electrolyte was an aqueous solution (250 mL) containing cupric sulfate (0.4 M) and lactic acid (3 M), after adjusting to pH = 9 by addition of aqueous NaOH (6 M, *ca.* 60 mL). The electrochemical deposition process was performed at a voltage of −0.40 V (*vs.* Ag/AgCl) at 60 °C for 30 min. The resulting CuO(NWA)|Cu_2O(NPy) (or Cu_2O(NPy)) photoelectrodes were obtained after washing with deionized water and drying under a flow of nitrogen.

2.2.3. Electrodeposition of metal nanoparticles

Noble metal (Ag or Au) nanoparticles were electrodeposited in a three-electrode cell (see 2.2.2) by using CuO(NWA) or CuO(NWA)|Cu_2O(NPy) as the working electrodes, Ag/AgCl as the reference electrode, and platinum sheet as the counter electrode. The electrodepositions were conducted in aqueous $NaNO_3$ (0.1 M) as supporting electrolyte, containing the desired metal precursor ($HAuCl_4$ or $AgNO_3$, 2 mM or 20 mM) in the dark for short lapses of time (typically 5 s, unless otherwise stated) at –0.20 V *vs.* Ag/AgCl. After rinsing with deionized water and drying under nitrogen gas, the metal-decorated CuO(NWA)|Ag, CuO(NWA)|Cu_2O(NPy)|Ag, CuO(NWA)|Au or CuO(NWA)|Cu_2O(NPy)|Au photoelectrodes were obtained.

2.3. Characterisation

X-ray diffraction of photoelectrode surfaces was performed on a

Bruker D8-ADVANCE instrument equipped with Cu-Kα radiation source. Raman spectra were obtained by using a Renishaw inVia Raman microscope equipped with a 514 nm laser. The morphology and the elemental distribution of photoelectrode surfaces were investigated by field-emission scanning electron microscopy (FESEM) using a Scios 2-FEI microscope equipped with a NiCol (Non-Immersion Column) electron column with electrostatic lenses. Energy dispersive X-ray spectroscopy (EDS) analyses coupled to FESEM were performed on the same equipment. A JEOL F200 TEM ColdFEG operated at 200 kV was used to obtain high-resolution transmission electron microscopy (HRTEM) or scanning transmission electron microscopy (STEM) images, acquired with a Gatan OneView camera, a CMOS-based and optical fibre-coupled detector. STEM images were recorded in high-angle annular dark-field (HAADF) mode using the Gatan DigiScan3 scanning unit with a camera length of 250 mm. Samples were inserted in a JEOL beryllium double-tilt holder for energy dispersive x-ray spectroscopy (EDS). STEM-EDS mapping was recorded from an EDS Centurio detector (silicon drift) with an effective area of 100 mm^2 and 133 eV of energy resolution, and the resulting images processed with the JEOL Analysis software. Photoelectrode cross-section samples were prepared by etching specimens into lamellae with a focused ion beam (FIB) in the FESEM instrument and then imaged by HRTEM.

2.4. Photoelectrochemical CO_2 reduction experiments

The as-prepared photoelectrodes were used as photocathodes (1 × 2.5 cm^2) directly for either electrochemical (EC) or photoelectrochemical (PEC) reduction of CO_2. In all experiments, a glass H-type cell with three-electrode configuration (Ossila) and an irradiation borosilicate window was employed with Ag/AgCl reference electrode and the working electrode on the cathode compartment, whereas a Pt sheet counter electrode was employed on the anode compartment. Both compartments were separated by a proton exchange membrane (Nafion®). Electrolytes were $KHCO_3$ solutions (0.5 M) after purging with CO_2 (15 min). Irradiation in PEC experiments was carried out by using an LED array lamp (Ossila, simulated solar spectrum according to the AM1.5 G standard, wavelength range: 350–1050 nm). Irradiances at the photoelectrode surfaces were ≈ 100 mW cm^{-2} (measured using a calibrated reference photodiode sensor by mks Ophir) by adjusting the distance to the light source. The linear sweep voltammetry (LSVs) measurements and chronoamperometry experiments during photoelectrochemical CO_2 reduction reaction were carried out using an Autolab PGSTAT101 Metrohm potentiostat/galvanostat with NOVA 2.1.6 software. Liquid samples (540 μL) were mixed with a standard potassium hydrogenphthalate solution in D_2O (5 mM, 60 μL) and analysed by ^1H nuclear magnetic resonance (^1H NMR) on a Bruker Avance Neo 400 MHz instrument for the quantification of CO_2 reduction products [6]. Each experiment was performed using a freshly prepared photoelectrode, and hence, single product analyses are reported. For transient photocurrent measurements, the photocathodes were subjected to chopped illumination at a constant potential (–0.4 V *vs.* Ag/AgCl) to record the photocurrent density graph over 10 s on/off irradiation (AM1.5 G, 350–1050 nm, 100 mW cm^{-2}) cycles.

3. Results and discussion

3.1. Structure and morphology of Cu_2O-CuO nanocomposites

The initial part of this work was devoted to adjusting the thermal oxidation parameters of copper sheets to optimise uniformity, surface density and length of cupric oxide nanowire arrays. Multiple synthetic conditions were explored and, for brevity, only systematic variations leading to successful results are reported herein. Specifically, mechanical stability, adhesion and resistance to flaking of the CuO nanowire layer were pursued. By varying the heating rate (≈ 25, 12 or 6 °C min^{-1}), it was found that slower heating ramps effectively promoted the growth of surface-dense and long nanowires, whereas the density and length of nanowires were decreased for faster rates (Fig. S1). Therefore, all subsequent Cu(NWA) preparations were carried out after 6 °C min^{-1} heating rates. Moreover, the effect of temperature was evaluated by performing the thermal oxidation procedure at 500 °C; since a lower nanowire density was achieved under those conditions (Fig. S1), the selected temperature for all subsequent preparations of CuO(NWA) materials was 400 °C. The CuO nanowire morphology was confirmed by top-view FESEM images, as shown in Fig. 1a, whereas cross-section images of the entire layer derived from thermal oxidation showed the expected underlying Cu_2O sub-layer (Fig. S2). Conversely, electrodeposition on pristine copper sheets results in compact layers composed of Cu_2O nanopyramidal blocks, as observed by FESEM (Cu_2O(NPy), Fig. S3).

The following step in nanocomposite construction was the electrodeposition of Cu_2O on CuO(NWA), aiming at the formation of CuO@-Cu_2O heterojunctions, *i.e.* effective coating of CuO nanowires by Cu_2O nanopyramids. The resulting CuO(NWA)|Cu_2O(NPy) photoelectrodes were studied by FESEM, showing the presence of vertically oriented CuO nanowires coated with evenly-distributed Cu_2O nanocrystals, mostly in the form of nanopyramids or stacked as nanoprisms (Fig. 1b and Fig. S4). The thickness of the initial CuO nanowires is below 100 nm, whereas the final CuO@Cu_2O heteronanostructures, most often adopting the overall morphology of truncated prisms, grow wider up to 200–400 nm.

The chemical composition of the copper-based photocathodes was examined by Raman spectroscopy. The spectrum of CuO(NWA) exhibits three peaks at around 298 (strong), 343, and 629 cm^{-1} which correspond to the active vibration modes, namely Ag, B_1g and B_2g, respectively, of CuO (Fig. 2a) [54]. This is consistent with the expected formation of long CuO nanowires by thermal oxidation of copper, although the intermediate Cu_2O layer underneath [50] is not detected, probably due to shallow penetration of the laser radiation during measurement. Conversely, the spectrum of CuO(NWA)|Cu_2O(NPy) is markedly different, *i.e.* only peaks attributable to cuprous oxide are observed (Fig. 2a). In particular, peaks located at 145 and 217 cm^{-1} can be assigned to the inactive Raman and second-order overtone modes of Cu_2O, respectively, whereas broader signals at 415, 535 and 640 cm^{-1} further confirm the presence of the cuprous oxide. Given that no appreciable signals of the CuO nanowires remain observable, Raman spectroscopy suggests that electrodeposition causes their extensive coverage with a nascent Cu_2O layer, which in turn hampers detection of the underlying CuO by Raman.

The phase composition of the photoelectrodes was studied by XRD. As opposed to what was revealed by Raman spectroscopy, diffraction signals of similar intensities for both CuO and Cu_2O phases are clearly observed for CuO(NWA), in addition to sharp and intense Cu^0 peaks (Fig. 2b, and Fig. S5 for peak assignment). The presence of the three different phases confirms the formation of the thin (several microns) double layer consisting of an intermediate Cu_2O and outer CuO nanowire array layers. The XRD pattern of CuO(NWA)|Cu_2O(NPy) shows essentially the same signals, although the Cu_2O/CuO intensity ratio increased, in agreement with the electrodeposition of Cu_2O on the surface, creating the desired core@shell heteronanostructure, whereby the nanowires of CuO become effectively coated with Cu_2O nanopyramids. Conversely, direct electrodeposition on Cu sheets in the Cu^{2+}/lactate electrolyte system only results in the formation of crystalline Cu_2O (Fig. S5).

3.2. Structure and morphology of electrodeposited noble metal co-catalysts

Deposition of noble metal co-catalysts was performed by a final electrochemical procedure to investigate their effect on CO_2 reduction activity and selectivity. Specifically, electrodeposition was employed as a strategy to control the growth of metal nanostructures by tuning various electrochemical parameters, such as electrolyte composition,

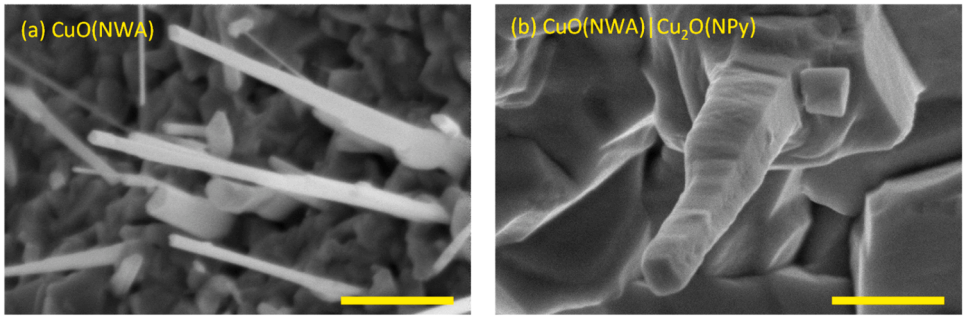

Fig. 1. FESEM images of (a) CuO(NWA) prepared by thermal oxidation (heating rates: 6 °C min^{-1}, then 400 °C for 3 h), and (b) CuO(NWA)|Cu_2O(NPy) synthesised by further electrodeposition (−0.4 V vs. Ag/AgCl), showing how the surface CuO nanowire arrays in the former become completely covered with Cu_2O nanopyramids or stacked nanoprisms; scale bars: 500 nm.

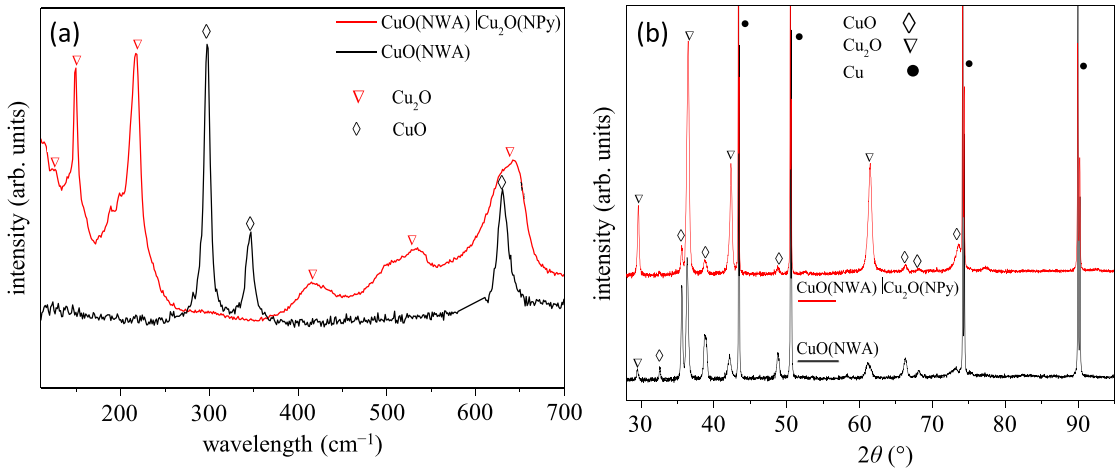

Fig. 2. Raman spectra (a) and X-ray diffractograms (b) of CuO(NWA) prepared by thermal oxidation, and of the derived CuO(NWA)|Cu_2O(NPy) material synthesised by further electrodeposition.

substrate surface, and applied potential. The electrochemical synthesis method offers capabilities for substrate-directed deposition routes of nanocatalysts in a controlled manner under mild cathodic potentials, for short periods of time and, in contrast to photodeposition methods, without the need to employ sacrificial electron donors.

The extent and mode of gold and silver electrodeposition on either CuO(NWA) or CuO(NWA)|Cu_2O(NPy) photoelectrodes depends on experimental parameters such as metallic precursor concentration, time, or surface texture. Increasing amounts of metallic silver or metallic gold on CuO(NWA) were loaded upon lengthening electrodeposition times, as observed by XRD (peaks at 38.0 and 38.2 °, respectively, Figs. S6 and S7), leading to CuO(NWA)|Ag photocathodes. The nanostructure of the photoelectrode also had a noticeable effect on the efficiency of noble metal electrodeposition. The amount of Ag^0 deposited on CuO(NWA)|Cu_2O(NPy) was significantly lower than on the parent CuO(NWA), as can be observed by XRD (Fig. 3).

The surface density and morphology of electrodeposited noble metals were further studied by FESEM. A clear increase in the amount of Ag^0 or Au^0 on the surfaces of CuO(NWA) was obvious upon lengthening electrodeposition times (Figs. S8 and S9). Essentially complete Ag^0 coverage occurred after only 5 s in the presence of $AgNO_3$ (20 mM), resulting in fern-like aggregates of nanocrystals formed by fast dendritic growth (Fig. S8a). The arborescent structures grew even thicker into complex platelet aggregates after longer electrodeposition times (20 s, Fig. S8b). Given that the motivation of this work was to deposit small amounts of noble metals as co-catalysts in order to minimise loading and prevent light-blocking to the photo-responsive copper oxide components, electrodeposition was tested in the presence of lower amounts of

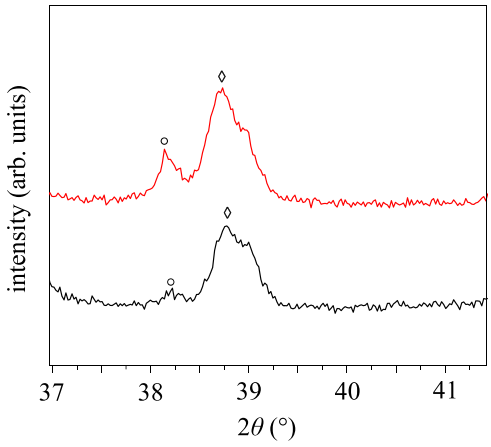

Fig. 3. Expanded XRD patterns of CuO(NWA)|Ag (red, top) and CuO(NWA)|Cu_2O(NPy)|Ag (black, bottom) photocathodes ([Ag^+] = 2 mM, −0.2 V vs. Ag/AgCl, 5 s), showing the typical (111) diffraction peaks for Ag and CuO at ca. 38.1 and 38.7 ° (circles and diamonds, respectively).

metallic precursors. On the one hand, $AgNO_3$ concentration was diminished by an order of magnitude (2 mM), resulting in spherical or plate-like aggregates of nanoparticles, mostly on the underlying flat surfaces rather than on CuO nanowires in CuO(NWA)|Ag, as confirmed by FESEM-EDS elemental mapping (sizes: 50–300 nm or up to ≈ 2 μm, Fig. S8c–f). Based on these initial experiments, optimised conditions

($[metal]_{aq}$ = 2 mM, t = 5 s), mostly leading to discrete Ag^0 aggregates, were set for all subsequent electrodeposition procedures. Favourable results were also obtained in the case of gold, whereby nanoparticles grew both around CuO nanowires and as spherical aggregates on flat surfaces to generate CuO(NWA)|Au photocathodes, yet evenly-dispersed in all cases (Fig. S9).

Noble metal electrodeposition on CuO(NWA)|Cu_2O(NPy) nanocomposites was pursued to complete the final nanocomposite photoelectrodes. Interestingly, the resulting morphologies were completely different to those obtained on CuO(NWA). Electrodeposited metallic silver nanoparticles on CuO(NWA)|Cu_2O(NPy)|Ag surfaces were exclusively and selectively arranged into continuous, albeit tortuous, nanotrails, mostly on flat parts of the surface, covered by Cu_2O nanopyramids (see FESEM images and derived EDS elemental distribution maps in Fig. 4a–c). On the contrary, the paths followed by nanotrails did not cover the CuO@Cu_2O heteronanostructures of stacked nanoprismatic morphology, but rather revolved around them (see overall and detailed views on Fig. S10). The Ag^0 nanotrails consisted of primary nanoparticles of sizes ranging 15–30 nm (see HRTEM images in Fig. S11), closely contacting each other into nanotrails of widths below 100 nm. The formation of nanotrails probably took place by sequential electrodeposition of individual Ag^0 nanoparticles upon electron accumulation onto the surfaces of previously formed ones. The case of gold was markedly different, that is, Au^0 electrodeposition resulted in scattered aggregates of nanoparticles on all areas of the surface of CuO(NWA)|Cu_2O(NPy)|Au photoelectrodes (see FESEM images and EDS elemental maps in Fig. 4d–f). Quite remarkably, noticeable accumulation of Au^0 nanoparticles was also observed onto the apexes of CuO(NWA)@Cu_2O nanopyramids or stacked nanoprisms (Fig. 4d). Primary Ag^0 particle size distribution can be described as bimodal given the existence of a fraction of smaller nanoparticles and another of slightly larger ones (2–6 and 10–20 nm, respectively, Fig. S11). In summary, the ternary CuO(NWA)|Cu_2O(NPy)|Ag and CuO(NWA)|Cu_2O(NPy)|Au nanocomposite photoelectrodes entailed the target morphology, *i.e.* partial coverage of metal nanoparticles to provide active reductive sites while allowing direct light impingement on the CuO@Cu_2O photo-responsive heteronanostructure.

3.3. Electrochemical stability studies

The stability of copper-based electrodes and photoelectrodes during CO_2 reduction is a matter deserving attention, especially with regards to phase stability, given that redox transformations between copper(II) and copper(I) oxides, and in addition with the metallic phase, may take place *in situ*, and are expected to greatly affect performance [36,55]. In this study, the electrochemical and photoelectrochemical stability of CuO (NWA) and CuO(NWA)|Cu_2O(NPy) was assessed with regards to morphology and phase composition changes.

Phase composition analyses of CuO(NWA) after treatment under conditions akin to electrochemical CO_2 reduction reactions at different potentials revealed noticeable evolution in all cases. Raman spectroscopy results indicate that CuO nanowires on the outer surface are prone to partial cathodic conversion via initial reduction to Cu_2O, even at the mildest potentials (noticeable increase in cuprous oxide signals at –0.2 V *vs.* Ag/AgCl, Fig. S12). More negative potentials resulted in the progressive disappearance of copper oxide signals due to total reduction. These results are complemented by XRD measurements, which provide an essentially comprehensive analysis of the copper oxide layers given their deeper penetration (Fig. S13). The intensity of Cu_2O diffraction signals clearly decreased after the electrochemical experiment at –0.2 V *vs.* Ag/AgCl, a fact that can be attributed to the reduction of the intermediate Cu_2O layer to Cu, whereas the diminution of the CuO signals is less apparent than what was observed in the corresponding Raman spectrum. However, more negative cathodic potentials caused faster reduction of CuO, probably to transient Cu_2O, as suggested by decreased and increased intensities of their respective signals after electrochemical treatment at –0.3 or –0.4 V. Progressive total reduction to Cu^0 took place at increasingly negative potentials, in agreement with Raman results above (Figs. S12, S13). In addition, FESEM images showed the formation of submicrocubes at –0.2 V, most likely Cu_2O, in parallel to the progressive disappearance of CuO nanowires. Harsher cathodic potentials lead to granular surface textures of metallic copper, with some presence of ill-defined nanowires that might have been formed by re-oxidation upon exposure to atmospheric oxygen (Fig. S14).

The CuO(NWA)|Cu_2O(NPy) nanostructures formed upon copper electrodeposition on CuO (NWA) exhibited a greatly enhanced cathodic stability, as indicated by Raman spectroscopy (Fig. S15). The Cu_2O/CuO signal intensity ratio remained essentially constant down to a potential

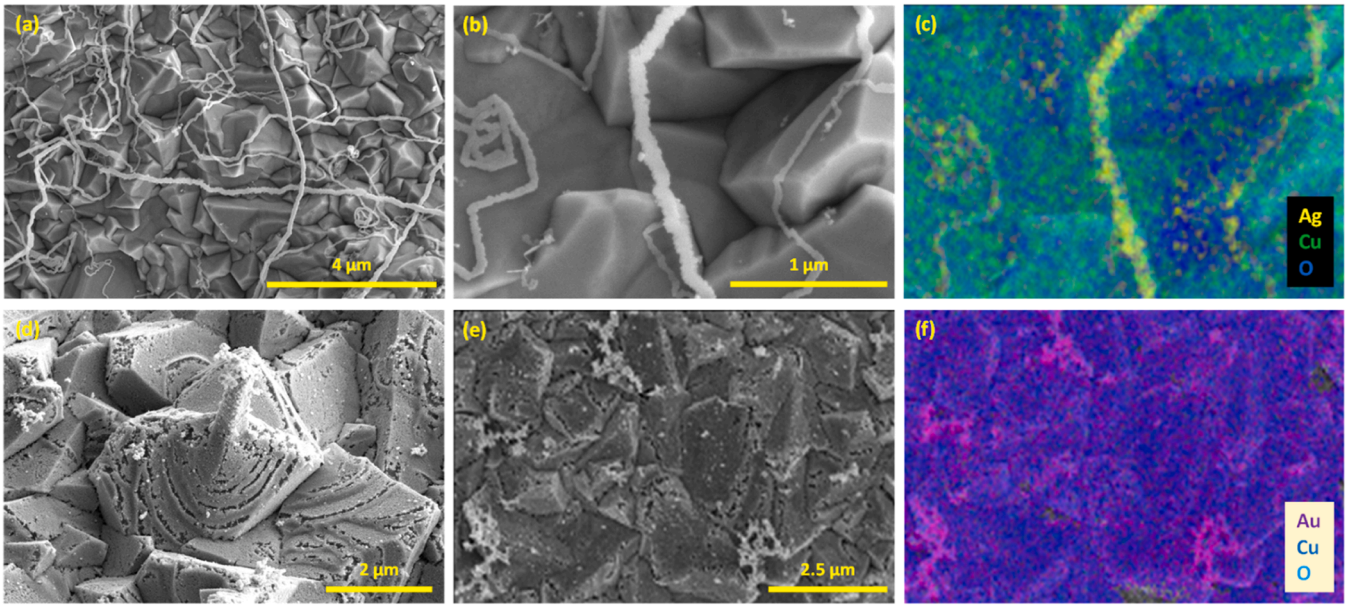

Fig. 4. FESEM (a,b,d,e) micrographs and FESEM-EDS elemental mapping images (c,f, corresponding to b,e) of CuO(NWA)|Cu_2O(NPy)|Ag (a–c) and CuO(NWA)|Cu_2O(NPy)|Au (d–f). Nanoparticles are arranged into silver nanotrails and gold nanoaggregates, respectively.

of –0.7 V, whereas only weak peaks for Cu_2O remained at more negative potential. Similar observations can be drawn from XRD analysis, which indicate extensive reduction to metallic copper at increasingly negative potentials (Fig. S16). Regarding morphology, this nanocomposite structure was maintained even at very negative potential of around –1 V, proving the enhanced electrochemical stability of CuO(NWA) after coating with a Cu_2O overlayer, that is, the core@shell CuO@Cu_2O nanostructures in CuO(NWA)|Cu_2O(NPy) (Fig. S17).

3.4. Photocurrent measurements

The photoelectrochemical properties of the prepared nanocomposite photoelectrodes were initially assessed by chronoamperometry under dark-irradiation cycles, thus obtaining insight into their photocurrent behaviour. Firstly, light response at –0.4 V (*vs.* Ag/AgCl) of nanocomposite CuO(NWA)|Cu_2O(NPy) was compared to that in the single-component parent CuO(NWA) photoelectrodes, showing a higher stability for the former, as opposed to increasing currents due to reduction of the constituent CuO(NWA) and Cu_2O (NPy) (Fig. S18). Remarkably, above three-fold current density increases (higher than 0.2 mA cm^{-2}) were recorded upon simulated sunlight irradiation for CuO(NWA)|Cu_2O(NPy) as compared to dark conditions. The photoelectrochemical CO_2 reduction activity was then tested by comparing the behaviour of CuO(NWA)|Cu_2O(NPy) in the presence or absence of CO_2. As observed in Fig. 5a, photocurrents were noticeably higher under CO_2 as compared to inert conditions (despite a marginally lower dark current), *i.e.* around 70 % higher than those in the N_2-saturated electrolyte. The effect of noble metal co-catalyst incorporation on photoelectrochemical reduction of CO_2 was also investigated (Fig. 5b,c). Interestingly, the dark-bright photocurrent change was significantly smaller for both CuO(NWA)|Cu_2O(NPy)|Ag and CuO(NWA)|Cu_2O(NPy)|Au nanocomposite photoelectrodes as compared to CuO(NWA)|Cu_2O(NPy), possibly indicating a light-blocking effect of the noble metal nanoparticle deposits on the surface of the photo-responsive Cu_2O layer. Moreover, noticeable differences are apparent for both metals in terms of current. In the case of silver, absolute current densities after multiple cycles were around 0.2 mA cm^{-2}, less than half those for CuO(NWA)|Cu_2O(NPy) (Fig. 5b). Conversely, gold enabled significantly higher absolute currents that progressively decreased to a steady regime above 0.5 mA cm^{-2} (Fig. 5c). Based on these results, it can be inferred that gold co-catalyst promotes more efficiently the transfer of charge carriers, notwithstanding less favourable activity upon light irradiation.

The effect of light on CuO(NWA)|Cu_2O(NPy) was also investigated by LSV measurements at cathodic potentials under conditions analogous to those of CO_2 photoelectrochemical reduction experiments, confirming the enhanced photocurrent trend described above (Fig. S19). Whilst dark currents remain nearly negligible down to −0.8 V, irradiation promotes cathodic events at significantly less demanding potentials (≤ −0.4 V). Moreover, the onset potential was also shifted to less negative values in the presence of carbon dioxide, indicating higher reductive activity upon increasing its partial pressure, and hence, its availability on the photocathode surface. Based on these observations, the prepared photocathodes were tested at −0.4 V in all (photo)electrochemical testing to ensure nanostructure stability.

3.5. Electro- and photoelectrochemical CO_2 reduction

Both electrochemical and photoelectrochemical CO_2 reduction experiments were performed on the designed nanocomposite photocathodes at mildly negative potentials (−0.4 V) to evaluate their activity while minimising structural and morphological changes upon operation. Product analyses in both liquid and gaseous samples were undertaken. Under the applied conditions, liquid-phase products were predominant, whereas only traces of hydrogen and carbon monoxide were detected in the gas phase. Therefore, productivities and selectivities were determined based on the main products identified by ^{1}H MNR in liquid samples (see Section 2.4), namely formate, acetate and methanol (Fig. 6 and Table S1). The data indicate that formate was the major CO_2 reduction product for all photocathodes, both in the presence and in the absence of light. Therefore, one plausible mechanistic assumption could be initial transformation of carbon dioxide (and/or aqueous

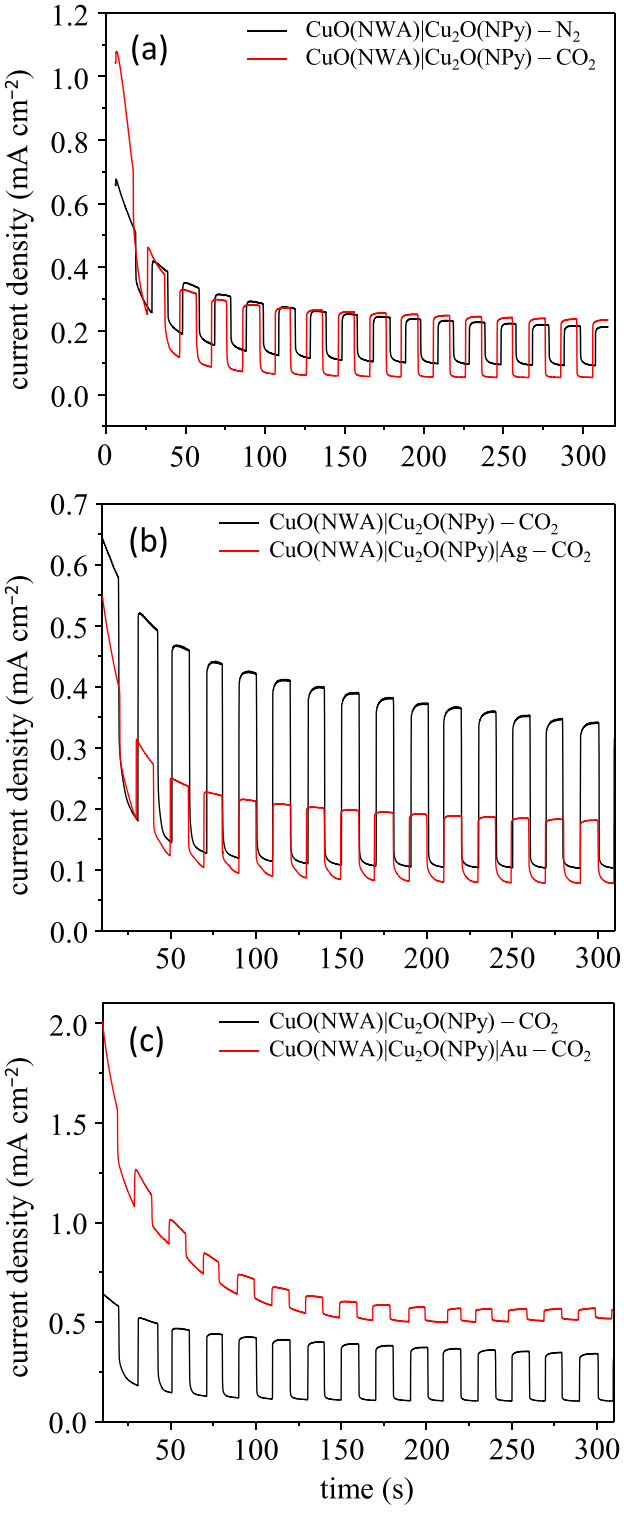

Fig. 5. Photocurrents recorded by chronoamperometry at –0.4 V vs. Ag/AgCl in $KHCO_3$ (0.5 M) under chopped simulated sunlight irradiation (LED light source, AM1.5 G, 100 mW cm^{-2}) on (a) CuO(NWA)|Cu_2O(NPy) photoelectrodes under N_2 or CO_2, comparison of CuO(NWA)|Cu_2O(NPy)|Ag (b) and CuO(NWA)|Cu_2O(NPy)|Au (c) relative to CuO(NWA)|Cu_2O(NPy) under CO_2.

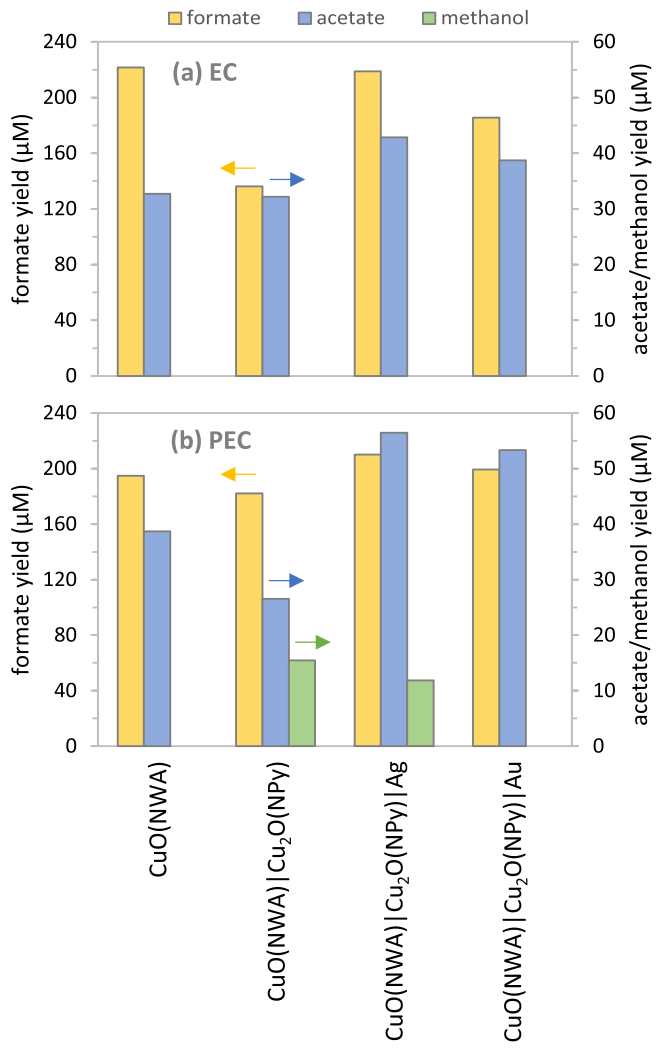

Fig. 6. Yields of CO_2 reduction products from electrochemical (a, EC) and photoelectrochemical (b, PEC) experiments. Experimental conditions: $KHCO_3$ (0.5 M), CO_2 atmosphere (1 bar), −0.4 V (vs. Ag/AgCl), simulated sunlight irradiation by LED light source (in b, PEC, AM1.5 G, 100 mW cm^{-2}), 2 h. Product analysis: liquid samples (540 μL) mixed with potassium hydrogenphthalate standard solution in D_2O (5 mM, 60 μL), ^1H NMR (400 MHz).

hydrogencarbonate) into formate as the primary product by a two electron/two proton, and essentially dark, process. Further reduction via multiple stages took place, as indicated by the formation of acetate. In purely electrochemical processes, no other carbon products were detected (Fig. 6a). The formation of copper oxide heterojunctions in the CuO(NWA)|Cu_2O(NPy) nanocomposite resulted in an apparently lower activity, despite its enhanced photostability as compared to the pristine CuO(NWA). Conversely, the deposition of noble metal co-catalysts marginally promoted the production of acetate. The CuO(NWA)|Cu_2O(NPy)|Ag photocathode, whereby silver nanotrails were present on the Cu_2O layer (see Section 3.2 and Fig. 4), led to the highest electrochemical acetate productivity (43 μM, Fig. 6a).

By performing analogous experiments in the presence of simulated sunlight, reaction outcomes were slightly different despite the consistent production of formate in similar quantities in all cases (Fig. 6b and NMR spectra in Fig. S20). The formation of acetate was also significant, especially in the photocathodes with noble metal co-catalysts. Noticeable 30–40 % increases in acetate production were observed for CuO(NWA)|Cu_2O(NPy)|Ag and CuO(NWA)|Cu_2O(NPy)|Au (up to 56 and 54 μM, respectively). This was not detrimental to formate yields, thus suggesting that photo-generated charges contributed to the overall redox process with additional productivity. The nanocomposite CuO(NWA)|Cu_2O(NPy) photocathode displayed lower acetate production as compared to all other counterparts and to the dark electrochemical reaction, but interestingly, resulted in formation of methanol with the highest recorded yield (> 15 μM, Fig. 6b and Table S1). This implies that the core@shell heterojunction of copper oxides, whereby CuO nanowires are covered with Cu_2O nanopyramids, provides effective electron migration routes toward suitable surface sites for multi-electron transfer, thus protecting against photocorrosion and enabling reduction into methanol. In addition to the remarkable acetate production recorded, the silver co-catalyst also enables the formation of methanol. These results represent outstanding production of oxygenates. The significant photoelectrochemical reduction of CO_2 into carboxylates, chiefly formate, but also acetate, has been achieved at remarkably mild potentials (−0.4 V *vs.* Ag/AgCl), as compared to related examples in the literature. Other systems based on Cu_2O leading to similar product distributions required much more negative potentials (−1.5 V *vs.* Ag/AgCl) [20]. Production of acetate has been reported on Cu_2O(NW)/Ag photoelectrodes also at slightly more cathodic potentials [32], whereas the positive effect of silver co-catalysts on acetate production as a single product has been also previously reported [30,31]. These and other literature data are compiled in Table S2 for comparison. The stability of the materials after photoelectrochemical CO_2 reduction was checked by XRD, showing that phase composition was essentially maintained (Fig. S21), despite minor changes such as a slight broadening of some copper oxide signals in CuO(NWA)|Cu_2O(NPy)|Au, probably indicating some decrease in crystallinity, a fact that will be further studied in upcoming research.

Based on the range and yields of products formed, a plausible CO_2 reduction mechanism is postulated for the nanocomposite photocathodes studied (Fig. 7a). As anticipated above, the prevalent generation of formate is consistent with a 2 e^-/2 H^+ initial reduction step. The carboxyl species thus formed may become protonated into formate, which would be readily desorbed and accumulate in the electrolyte as the major liquid-phase product, also in the dark. Further reduction of the adsorbed carboxyl with ensuing deoxygenation is expected to lead to formyl intermediates. Since no formaldehyde or related products were detected, it is reasonable to hypothesise that subsequent reduction is favoured on the photocathode surface. A further 2 e^-/2 H^+ reduction step resulting in hydroxymethyl, that may then desorb with protonation into methanol, is proposed. This step might require additional charge carrier generation, driven by irradiation, as discussed below. The remarkable acetate yields from our photocathodes can be rationalised as the outcome of C–C coupling events between adsorbates, especially in the presence of noble metal co-catalysts. One possibility is a nucleophilic attack of the initially formed carboxylate onto hydroxymethyl, with water elimination upon protonation of hydroxyl. Acetate can be then released into the aqueous medium after protonation. Other possible pathways leading to acetate would be the reduction of hydroxymethyl into methyl and its carboxylation with CO_2 (Fig. 7a), or the coupling of CO with methyl radicals promoted by Ag or Au [12,13]. In summary, the formation, stabilisation and further transformation of intermediates such as carboxylate, hydroxymethyl and/or methyl species on copper oxide surface sites might play key roles in the efficient CO_2 reduction processes observed.

The greatly improved (photo)electrochemical stability of the CuO@Cu_2O, core@shell, nanostructure of the CuO(NWA)|Cu_2O(NPy) photocathodes with respect to bare CuO nanowires on the interlayer can be rationalised in terms of charge carrier transport phenomena, as briefly discussed in Section 3.3. A postulation of the charge transfer phenomena taking place between the different photocathode constituents during photoelectrochemical CO_2 reduction is depicted in Fig. 7b. Due to the electrical bias applied, electrons flow towards the photocathode and through the Cu^0 sheet underlayer into the nanocomposite formed by copper oxide phases. The intermediate Cu_2O layer firstly accepts electrons, and as a p-type semiconductor, it may promote their

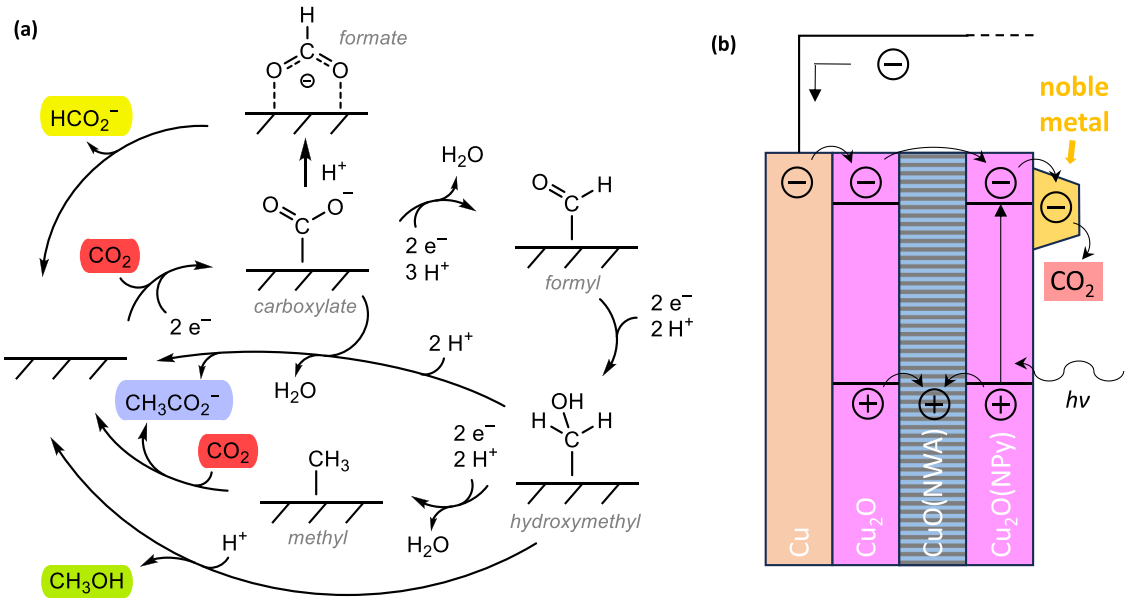

Fig. 7. Mechanistic proposal of the (photo)electrochemical CO_2 (or hydrogencarbonate derived thereof) reduction process on the studied photocathodes. (a) Plausible catalytic cycles leading to the formation of the observed products, i.e. formate, acetate and methanol; most intermediates are depicted as C–bonded adsorbates, although their evolution into O–bonded counterparts cannot be ruled out. (b) Possible flow directions of charge carriers driven by either potential bias or light, whereby excess holes on p-type Cu_2O may prevent CuO corrosion by reduction, and electrons are transferred via noble metal co-catalysts into CO_2.

annihilation with its existing majority carriers, *i.e.* holes. Excess electrons might migrate through the heterojunctions toward the surface and participate in the reduction of CO_2 (or HCO_3^-, or any intermediates shown in Fig. 7a) on active sites on Cu_2O or on noble metal nanoparticles. Conversely, the predominance of majority holes in Cu_2O might partly migrate into the CuO nanowires, minimising its tendency to be reduced under cathodic potentials, and hence, preventing corrosion (see Section 3.3). Under irradiation, an additional and more direct route to reduction is established after promotion of electrons upon photonic absorption by the outer Cu_2O nanopyramid layer, whereas photogenerated holes left behind may contribute to the corrosion inhibition effect on CuO (Fig. 7b). This light-induced charge carrier generation and accumulation is beneficial to promote multi-electron reduction processes, leading to enhanced production of acetate and methanol.

4. Conclusions

Control of the nanostructure of multi-junction copper-based photocathodes has been undertaken by adjusting synthetic conditions in order to maximise electrochemical stability and CO_2 reduction activity. In particular, CuO nanowires on Cu_2O, formed upon thermal oxidation of Cu sheets, have been covered with an additional uniform layer of Cu_2O nanopyramids and stacked nanoprisms by electrodeposition (CuO (NWA)|Cu_2O(NPy)). The thereby adequately and intimately formed core@shell CuO@Cu_2O nanostructures greatly improved electrochemical stability up to –0.7 V (*vs.* Ag/AgCl), whilst bare CuO nanowires rapidly disappeared by reduction into Cu_2O and Cu^0 at similar potentials. This is most likely due to the effective transfer of electrons by reduction-active p-type cuprous oxide surfaces, and to the accumulation of majority holes in the bulk, which can migrate to CuO across the heterojunction and minimise its reduction. Furthermore, the effect of noble metals on CO_2 reduction activity was tested after electrochemically loading small amounts of Ag or Au co-catalysts on the surfaces of CuO(NWA)|Cu_2O(NPy). Formate was readily formed on all studied photocathodes, whereas acetate production was enhanced in the presence of the noble metal co-catalysts, especially Ag. An additional promoting effect due to simulated sunlight irradiation was observed; photoelectrochemical acetate yields increased by 30–40 % for CuO (NWA)|Cu_2O(NPy)|Ag and CuO(NWA)|Cu_2O(NPy)|Au up to 56 and 54 μM, respectively. Methanol was also identified as a product by photoelectrochemical CO_2 reduction on CuO(NWA)|Cu_2O(NPy) and CuO (NWA)|Cu_2O(NPy)|Ag.

CRediT authorship contribution statement

Tahereh Mokary Yazdely: Data curation; Formal analysis; Investigation; Methodology; Writing – Original draft. **Ricard Garcia-Valls:** Conceptualization; Formal analysis; Project administration; Resources; Supervision; Writing – Review & editing. **Alberto Puga:** Conceptualization; Data curation; Formal analysis; Funding acquisition; Investigation; Methodology; Project administration; Resources; Supervision; Validation; Writing – Original draft; Writing – Review & editing.

Declaration of Competing Interest

The authors declare the following financial interests/personal relationships which may be considered as potential competing interests: Alberto Puga reports financial support was provided by State Agency of Research. If there are other authors, they declare that they have no known competing financial interests or personal relationships that could have appeared to influence the work reported in this paper.

Acknowledgments

This work is part of Grant PID2020–116322RB-C32 funded by the Spanish Research State Agency (Agencia Estatal de Investigación, MICIU/AEI/10.13039/501100011033). T.M. thanks Universitat Rovira i Virgili for a pre-doctoral contract (2020MFP-COFUND-26) within its *Marti i Franquès* COFUND Fellowship programme. The TEM instrument was partially funded by the operative program *FEDER Catalunya* 2014-2020 (IU16-015844). Dr. S. Plana is gratefully acknowledged for useful discussions on TEM results.

Appendix A. Supporting information

Supplementary data associated with this article can be found in the online version at doi:10.1016/j.nxnano.2024.100125.

References

[1] E.V. Kondratenko, G. Mul, J. Baltrusaitis, G.O. Larrazábal, J. Pérez-Ramírez, Status and perspectives of CO_2 conversion into fuels and chemicals by catalytic, photocatalytic and electrocatalytic processes, Energy Environ. Sci. 6 (2013) 3112–3135, https://doi.org/10.1039/C3EE41272E.

[2] W. Gao, S. Liang, R. Wang, Q. Jiang, Y. Zhang, Q. Zheng, B. Xie, C.Y. Toe, X. Zhu, J. Wang, L. Huang, Y. Gao, Z. Wang, C. Jo, Q. Wang, L. Wang, Y. Liu, B. Louis, J. Scott, A.-C. Roger, R. Amal, H. He, S.-E. Park, Industrial carbon dioxide capture and utilization: state of the art and future challenges, Chem. Soc. Rev. (2020), https://doi.org/10.1039/D0CS00025F.

[3] Global Hydrogen Review 2023, International Energy Agency, Paris, 2023..

[4] M. Aresta, A. Dibenedetto, A. Angelini, Catalysis for the valorization of exhaust carbon: from CO_2 to chemicals, materials, and fuels. TechnologicaL Use of CO_2, Chem. Rev. 114 (2014) 1709–1742, https://doi.org/10.1021/cr4002758.

[5] R. Kortlever, J. Shen, K.J.P. Schouten, F. Calle-Vallejo, M.T.M. Koper, Catalysts and reaction pathways for the electrochemical reduction of carbon dioxide, J. Phys. Chem. Lett. 6 (2015) 4073–4082, https://doi.org/10.1021/acs.jpclett.5b01559.

[6] P. Preikschas, A.J. Martín, B.S. Yeo, J. Pérez-Ramírez, NMR-based quantification of liquid products in CO_2 electroreduction on phosphate-derived nickel catalysts, Commun. Chem. 6 (2023) 147, https://doi.org/10.1038/s42004-023-00948-9.

[7] S. Yoshino, T. Takayama, Y. Yamaguchi, A. Iwase, A. Kudo, CO_2 reduction using water as an electron donor over heterogeneous photocatalysts aiming at artificial photosynthesis, Acc. Chem. Res. (2022), https://doi.org/10.1021/acs.accounts.1c00676.

[8] Skillen N., Robertson P.K.J., Artificial Photosynthesis, in: Sol. Energy, pp. 205-241.

[9] M. Bonchio, J. Bonin, O. Ishitani, T.-B. Lu, T. Morikawa, A.J. Morris, E. Reisner, D. Sarkar, F.M. Toma, M. Robert, Best practices for experiments and reporting in photocatalytic CO2 reduction, Nat. Catal. 6 (2023) 657–665, https://doi.org/10.1038/s41929-023-00992-7.

[10] V. Kumaravel, J. Bartlett, S.C. Pillai, Photoelectrochemical conversion of carbon dioxide (CO2) into fuels and value-added products, ACS Energy Lett. 5 (2020) 486–519, https://doi.org/10.1021/acsenergylett.9b02585.

[11] S. Nitopi, E. Bertheussen, S.B. Scott, X. Liu, A.K. Engstfeld, S. Horch, B. Seger, I.E. L. Stephens, K. Chan, C. Hahn, J.K. Nørskov, T.F. Jaramillo, I. Chorkendorff, Progress and perspectives of electrochemical CO_2 reduction on copper in aqueous electrolyte, Chem. Rev. 119 (2019) 7610–7672, https://doi.org/10.1021/acs.chemrev.8b00705.

[12] D. Gao, R.M. Arán-Ais, H.S. Jeon, B. Roldan Cuenya, Rational catalyst and electrolyte design for CO_2 electroreduction towards multicarbon products, Nat. Catal. 2 (2019) 198–210, https://doi.org/10.1038/s41929-019-0235-5.

[13] H. Liang, M. Li, Z. Li, W. Xie, T. Zhang, Q. Wang, Photoelectrochemical CO_2 reduction with copper-based photocathodes, J. CO_2 Util. 79 (2024) 102639, https://doi.org/10.1016/j.jcou.2023.102639.

[14] K. Wang, Y. Ma, Y. Liu, W. Qiu, Q. Wang, X. Yang, M. Liu, X. Qiu, W. Li, J. Li, Insights into the development of Cu-based photocathodes for carbon dioxide (CO_2) conversion, Green. Chem. 23 (2021) 3207–3240, https://doi.org/10.1039/D0GC04417B.

[15] P. Wang, S. Wang, H. Wang, Z. Wu, L. Wang, Recent progress on photo-electrocatalytic reduction of carbon dioxide, Part. Part. Syst. Charact. 35 (2018) 1700371, https://doi.org/10.1002/ppsc.201700371.

[16] S. Sun, X. Zhang, Q. Yang, S. Liang, X. Zhang, Z. Yang, Cuprous oxide (Cu_2O) crystals with tailored architectures: a comprehensive review on synthesis, fundamental properties, functional modifications and applications, Prog. Mater. Sci. 96 (2018) 111–173, https://doi.org/10.1016/j.pmatsci.2018.03.006.

[17] Z. Zhao, H. Wang, Q. Yu, S. Roy, X. Yu, Photo-/electrocatalytic approaches to CO_2 conversion on Cu_2O-based catalysts, Appl. Catal. A Gen. 667 (2023) 119445, https://doi.org/10.1016/j.apcata.2023.119445.

[18] M. Xia, L. Pan, Y. Liu, J. Gao, J. Li, M. Mensi, K. Sivula, S.M. Zakeeruddin, D. Ren, M. Grätzel, Efficient Cu_2O photocathodes for aqueous photoelectrochemical CO_2 reduction to formate and syngas, J. Am. Chem. Soc. 145 (2023) 27939–27949, https://doi.org/10.1021/jacs.3c06146.

[19] M.B. Akbar, Y. Wang, X. Zhang, T. He, Study on photoelectrochemical CO_2 reduction over Cu2O, J. Photochem. Photobiol. A Chem. 437 (2023) 114483, https://doi.org/10.1016/j.jphotochem.2022.114483.

[20] J.F. de Brito, C. Genovese, F. Tavella, C. Ampelli, M.V. Boldrin Zanoni, G. Centi, S. Perathoner, CO_2 reduction of hybrid Cu_2O–Cu/gas diffusion layer electrodes and their integration in a Cu-based photoelectrocatalytic cell, ChemSusChem 12 (2019) 4274–4284, https://doi.org/10.1002/cssc.201901352.

[21] Y. Zhang, W. Qiu, Y. Liu, K. Wang, W. Li, J. Kang, X. Qiu, M. Liu, W. Li, J. Li, Modulating the Cu_2O photoelectrode/electrolyte interface with bilayer surfactant simulating cell membranes for boosting photoelectrochemical CO_2 reduction, J. Phys. Chem. Lett. 14 (2023) 6301–6308, https://doi.org/10.1021/acs.jpclett.3c00672.

[22] S.Y. Oh, D.S. Kim, H.H. Lee, K.W. Lee, J.H. Choi, W.S. Yang, Y.S. Choi, D.W. Kim, J. W. Byeon, H.S. Lee, H.K. Cho, Exactly regulated copper catalysts exploiting isolated photoelectrochemical reduction of cuprous oxides and random mesh-structured TiO_2 for enhanced photoelectrochemical CO_2 conversion, J. Mater. Chem. A (2024), https://doi.org/10.1039/D4TA01486C.

[23] Q. Zhou, Y. Chen, H. Shi, R. Chen, M. Ji, K. Li, H. Wang, X. Jiang, C. Lu, The construction of p/n-Cu_2O heterojunction catalysts for efficient CO_2 photoelectric reduction, Catalysts 13 (2023) 857.

[24] H.-Y. Kang, D.-H. Nam, K.D. Yang, W. Joo, H. Kwak, H.-H. Kim, S.-H. Hong, K. T. Nam, Y.-C. Joo, Synthetic mechanism discovery of monophase cuprous oxide for record high photoelectrochemical conversion of CO_2 to methanol in water, ACS Nano 12 (2018) 8187–8196, https://doi.org/10.1021/acsnano.8b03293.

[25] L.J. Minggu, M.N.I. Salehmin, M.A. Mohamed, K. Arifin, R.M. Yunus, M.B. Kassim, A low overpotential photoelectrochemical reduction of carbon dioxide to methanol with highly photoactive hierarchical structured cuprous oxide, Ceram. Int. 46 (2020) 26004–26016, https://doi.org/10.1016/j.ceramint.2020.07.091.

[26] J.A.L. Perini, L.D.M. Torquato, J.Fd Brito, G.A. Andolpho, M.A. Gonçalves, L.D. De Angelis, L.D. Germano, S.I. Córdoba de Torresi, T.C. Ramalho, M.V.B. Zanoni, Solar-driven CO_2 conversion to methane and methanol using different nanostructured Cu_2O-based catalysts modified with Au nanoparticles, J. Energy Chem. 91 (2024) 287–298, https://doi.org/10.1016/j.jechem.2023.10.057.

[27] X. Chang, T. Wang, Z.-J. Zhao, P. Yang, J. Greeley, R. Mu, G. Zhang, Z. Gong, Z. Luo, J. Chen, Y. Cui, G.A. Ozin, J. Gong, Tuning Cu/Cu_2O interfaces for the reduction of carbon dioxide to methanol in aqueous solutions, Angew. Chem. Int. Ed. 57 (2018) 15415–15419, https://doi.org/10.1002/anie.201805256.

[28] P. Uthirakumar, H. Son, V. Dao, Y. Lee, S. Yadav, I.-H. Lee, Accelerating photoelectrochemical CO_2RR selectively of C_{2+} products by integrating Ag/Pd cocatalysts on Cu/Cu_2O/CuO heterojunction nanorods, J. Environ. Chem. Eng. 12 (2024) 112442, https://doi.org/10.1016/j.jece.2024.112442.

[29] M. Kan, C. Yang, Q. Wang, Q. Zhang, Y. Yan, K. Liu, A. Guan, G. Zheng, Defect-assisted electron tunneling for photoelectrochemical CO2 reduction to ethanol at low overpotentials, Adv. Energy Mater. 12 (2022) 2201134, https://doi.org/10.1002/aenm.202201134.

[30] E. Landaeta, R.A. Masitas, T.B. Clarke, S. Rafacz, D.A. Nelson, M. Isaacs, Z. D. Schultz, Copper-oxide-coated silver nanodendrites for photoelectrocatalytic CO_2 reduction to acetate at low overpotential, ACS Appl. Nano Mater. 3 (2020) 3478–3486, https://doi.org/10.1021/acsanm.0c00210.

[31] E. Landaeta, N.I. Kadosh, Z.D. Schultz, Mechanistic study of plasmon-assisted in situ photoelectrochemical CO_2 reduction to acetate with a Ag/Cu_2O nanodendrite electrode, ACS Catal. 13 (2023) 1638–1648, https://doi.org/10.1021/acscatal.2c05082.

[32] Y. Zhang, Q. Wang, K. Wang, Y. Liu, L. Zou, Y. Zhou, M. Liu, X. Qiu, W. Li, J. Li, Plasmonic Ag-decorated Cu_2O nanowires for boosting photoelectrochemical CO_2 reduction to multi-carbon products, Chem. Commun. 58 (2022) 9421–9424, https://doi.org/10.1039/D2CC03167A.

[33] P. Uthirakumar, Y. Lee, H. Son, V. Dao, C.Y. Kim, I.-H. Lee, Binder-free Cu/Cu_2O/CuO/Pd nanorods photoelectrode for regulating the faradaic efficiency for acetaldehyde and acetate production during photoelectrochemical CO_2RR by stabilizing the Cu_2O phase, J. Environ. Chem. Eng. 11 (2023) 111253, https://doi.org/10.1016/j.jece.2023.111253.

[34] X. Wang, C. Gao, J. Low, K. Mao, D. Duan, S. Chen, R. Ye, Y. Qiu, J. Ma, X. Zheng, R. Long, X. Wu, L. Song, J. Zhu, Y. Xiong, Efficient photoelectrochemical CO_2 conversion for selective acetic acid production, Sci. Bull. 66 (2021) 1296–1304, https://doi.org/10.1016/j.scib.2021.04.004.

[35] M. Melchionna, P. Fornasiero, M. Prato, M. Bonchio, Electrocatalytic CO_2 reduction: role of the cross-talk at nano-carbon interfaces, Energy Environ. Sci. 14 (2021) 5816–5833, https://doi.org/10.1039/D1EE00228G.

[36] S. Rej, M. Bisetto, A. Naldoni, P. Fornasiero, Well-defined Cu_2O photocatalysts for solar fuels and chemicals, J. Mater. Chem. A 9 (2021) 5915–5951, https://doi.org/10.1039/D0TA10181H.

[37] M.E. Aguirre, R. Zhou, A.J. Eugene, M.I. Guzman, M.A. Grela, Cu_2O/TiO2heterostructures for CO_2 reduction through a direct Z-scheme: protecting Cu_2O from photocorrosion, Appl. Catal. B Environ. 217 (2017) 485–493, https://doi.org/10.1016/j.apcatb.2017.05.058.

[38] M. Lu, D. Jia, H. Xue, J. Tian, T. Jiang, 0D/1D $CuFeO_2$/CuO nanowire heterojunction arrays for improved photoelectrocatalytic reduction of CO_2 to ethanol, J. Alloy. Compd. 960 (2023) 170626, https://doi.org/10.1016/j.jallcom.2023.170626.

[39] K. Lee, S. Lee, H. Cho, S. Jeong, W.D. Kim, S. Lee, D.C. Lee, Cu^+-incorporated TiO_2 overlayer on Cu_2O nanowire photocathodes for enhanced photoelectrochemical conversion of CO_2 to methanol, J. Energy Chem. 27 (2018) 264–270, https://doi.org/10.1016/j.jechem.2017.04.019.

[40] D.H. Won, C.H. Choi, J. Chung, S.I. Woo, Photoelectrochemical production of formic acid and methanol from carbon dioxide on metal-decorated CuO/Cu_2O-layered thin films under visible light irradiation, Appl. Catal. B Environ. 158-159 (2014) 217–223, https://doi.org/10.1016/j.apcatb.2014.04.021.

[41] J.-J. Velasco-Vélez, C.-H. Chuang, D. Gao, Q. Zhu, D. Ivanov, H.S. Jeon, R. Arrigo, R.V. Mom, E. Stotz, H.-L. Wu, T.E. Jones, B. Roldan Cuenya, A. Knop-Gericke, R. Schlögl, On the activity/selectivity and phase stability of thermally grown copper oxides during the electrocatalytic reduction of CO_2, ACS Catal. 10 (2020) 11510–11518, https://doi.org/10.1021/acscatal.0c03484.

[42] H. Son, J.-H. Lee, P. Uthirakumar, D. Van Dao, A. Soon, I.-H. Lee, Facile synthesis of flexible and scalable Cu/Cu_2O/CuO nanoleaves photoelectrodes with oxidation-induced self-initiated charge-transporting platform for photoelectrochemical water splitting enhancement, J. Alloy. Compd. 942 (2023) 169094, https://doi.org/10.1016/j.jallcom.2023.169094.

[43] L. Mai, X. Tian, X. Xu, L. Chang, L. Xu, Nanowire electrodes for electrochemical energy storage devices, Chem. Rev. 114 (2014) 11828–11862, https://doi.org/10.1021/cr500177a.

[44] N.P. Dasgupta, J. Sun, C. Liu, S. Brittman, S.C. Andrews, J. Lim, H. Gao, R. Yan, P. Yang, 25th anniversary article: semiconductor nanowires – synthesis, characterization, and applications, Adv. Mater. 26 (2014) 2137–2184, https://doi.org/10.1002/adma.201305929.

[45] Z. Wang, L. Xu, Y. Zhou, Y. Liang, J. Yang, D. Wu, S. Zhang, X. Han, X. Shi, J. Li, Y. Yuan, P. Deng, X. Tian, Stabilizing the oxidation state of catalysts for effective electrochemical carbon dioxide conversion, Chem. Soc. Rev. 53 (2024) 6295–6321, https://doi.org/10.1039/D3CS00887H.

[46] X. Jiang, T. Herricks, Y. Xia, CuO nanowires can be synthesized by heating copper substrates in air, Nano Lett. 2 (2002) 1333–1338, https://doi.org/10.1021/nl0257519.
[47] K. Rajeshwar, N.R. de Tacconi, G. Ghadimkhani, W. Chanmanee, C. Janáky, Tailoring copper oxide semiconductor nanorod arrays for photoelectrochemical reduction of carbon dioxide to methanol, ChemPhysChem 14 (2013) 2251–2259, https://doi.org/10.1002/cphc.201300080.
[48] P. Ding, T. Jiang, N. Han, Y. Li, Photocathode engineering for efficient photoelectrochemical CO_2 reduction, Mater. Today Nano 10 (2020) 100077, https://doi.org/10.1016/j.mtnano.2020.100077.
[49] T. Butburee, Y. Bai, J. Pan, X. Zong, C. Sun, G. Liu, L. Wang, Step-wise controlled growth of metal@TiO_2 core-shells with plasmonic hot spots and their photocatalytic properties, J. Mater. Chem. A 2 (2014) 12776–12784, https://doi.org/10.1039/C4TA01120A.
[50] J. Shi, L. Qiao, Y. Zhao, Z. Sun, W. Feng, Z. Zhang, J. Wang, X. Men, Synergistic effects on thermal growth of CuO nanowires, J. Alloy. Compd. 815 (2020) 152355, https://doi.org/10.1016/j.jallcom.2019.152355.
[51] L. Xiang, J. Guo, C. Wu, M. Cai, X. Zhou, N. Zhang, A brief review on the growth mechanism of CuO nanowires via thermal oxidation, J. Mater. Res. 33 (2018) 2264–2280, https://doi.org/10.1557/jmr.2018.215.
[52] P.E. de Jongh, D. Vanmaekelbergh, J.J. Kelly, Cu_2O: Electrodeposition and characterization, Chem. Mater. 11 (1999) 3512–3517, https://doi.org/10.1021/cm991054e.
[53] M.M. Elmahdy, A. El-Shaer, Structural, optical and dielectric investigations of electrodeposited p-type Cu_2O, J. Mater. Sci. Mater. Electron. 30 (2019) 19894–19905, https://doi.org/10.1007/s10854-019-02356-z.
[54] H.F. Goldstein, D.-s Kim, P.Y. Yu, L.C. Bourne, J.P. Chaminade, L. Nganga, Raman study of CuO single crystals, Phys. Rev. B 41 (1990) 7192–7194, https://doi.org/10.1103/PhysRevB.41.7192.
[55] H. Homayoni, W. Chanmanee, N.R. de Tacconi, B.H. Dennis, K. Rajeshwar, Continuous flow photoelectrochemical reactor for solar conversion of carbon dioxide to alcohols, J. Electrochem. Soc. 162 (2015) E115, https://doi.org/10.1149/2.0331508jes.